ELSEVIER

Physics of the Earth and Planetary Interiors 105 (1998) 59–71

PHYSICS OF THE EARTH AND PLANETARY INTERIORS

Thermal equation of state of garnets along the pyrope–majorite join

Yanbin Wang [a,b,*], Donald J. Weidner [a], Jianzhong Zhang [a], Gabriel D. Gwanmesia [c], Robert C. Liebermann [a]

[a] *Center for High Pressure Research and Department of Earth and Space Sciences, University at Stony Brook, Stony Brook, NY 11794-2100, USA*

[b] *Consortium for Advanced Radiation Sources, The University of Chicago, 5640 South Ellis Avenue, Chicago 60637, IL, USA*

[c] *Department of Physics and Astronomy, Delaware State University, Dover 19901, DE, USA*

Received 25 March 1997; received in revised form 2 June 1997; accepted 2 June 1997

Abstract

P–V–T relations of two garnet samples along the pyrope (Py)–majorite (Mj) join (Py_nMj_{1-n}, where subscripts indicate molar percent) were measured at pressure and temperature conditions up to 11 GPa and 1163 K, respectively, with energy-dispersive synchrotron X-ray diffraction in a cubic-anvil, DIA-6 type apparatus (SAM-85). For each volume measurement, non-hydrostatic stress was determined from relative shifts of the diffraction lines of NaCl, within which the sample was embedded. Heating to ~ 1100 K reduced the strength of NaCl below 0.1 GPa, making the measurements nearly hydrostatic. The recovered samples were examined by transmission electron microscopy (TEM) to detect irreversible changes that may affect data quality. For the cubic garnet $Py_{62}Mj_{38}$, no irreversible changes took place during the experiment. A fit using the third-order Birch–Murnaghan equation of state yielded ambient cell volume $V_0 = 1509.2(3)$ Å^3 (113.62 cc/mol), isothermal bulk modulus $K_{T0} = 160(3)$ GPa, and its pressure derivative $K'_{T0} = 4.9(5)$. Various thermal equations-of-state analyses gave consistent results for the temperature derivative of bulk modulus $(\partial K_T/\partial T)_P = -0.020(1)$ GPa K^{-1}, pressure derivative for thermal expansion $(\partial\alpha/\partial P)_T = -7.8 \times 10^{-7}$ GPa^{-1} K^{-1}, with the ambient volumetric thermal expansion $\alpha_0 = 2.5 \times 10^{-5}$ K^{-1}. For the tetragonal sample $Py_{21}Mj_{79}$, TEM indicated that micro-twin domains were significantly coarsened after the P–V–T experiment. Stress relaxation may have occurred during the coarsening, thereby compromising the P–V–T data. In addition, the tetragonal distortion in this sample was too small to be resolved by the energy-dispersive technique. Therefore, data for the latter sample were not suitable for accurate equation-of-state analysis. Previous data on pyrope were compiled, analyzed, and compared with the new data on the majoritic garnet. The entire data set enabled us to examine systematics of the thermoelastic properties of garnets along the majorite–pyrope join. These data will have important applications for modeling the transition zone of the mantle. Published by Elsevier Science B.V.

Keywords: Mineral physics; Equation of state; High pressure behavior; X-ray diffraction; Majorite; Transition zone; Composition of the mantle

* Corresponding author.

0031-9201/98/$19.00 Published by Elsevier Science B.V.
PII S0031-9201(97)00072-1

1. Introduction

Mineral physics constraints on composition models of the Earth's mantle rely on knowledge of thermal equations of state of candidate minerals. Recently, such pressure (P)–volume (V)–temperature (T) data have been obtained for most high-pressure phases of silicates, e.g., β- and γ-$(Mg,Fe)_2SiO_4$, and $CaSiO_3$- and $MgSiO_3$-perovskites (Fei et al., 1992a; Meng et al., 1993, 1994; Wang et al., 1994, 1996). Garnets as an important group of minerals in the transition zone and upper portion of the lower mantle have not been studied extensively in terms of P–V–T relations. Petrological studies indicate that the solubility of pyroxene in garnet increases rapidly with pressure and temperature and that majorite garnet (i.e., garnet structured pyroxene–garnet solid solution with octahedrally-coordinated Si) forms in a wide compositional range above 15 GPa (e.g., Akaogi and Akimoto, 1977; Kanzaki, 1987; Gasparik, 1989, 1990). Elements such as Ca, Fe, and Al are easily incorporated into the garnet structure and tend to widen P–T the stability field of majoritic garnet (e.g., Gasparik, 1996).

Elastic moduli of majorite garnets have been measured using Brillouin-scattering and ultrasonic techniques at ambient conditions (e.g., Bass and Kanzaki, 1990; Yeganeh-Haeri et al., 1990; Pacalo and Weidner, 1996; Sinogeikin et al., 1996). Acoustic measurements are available for a majorite–garnet sample with 62 mol% pyrope and 38 mol% majorite ($Py_{62}Mj_{38}$) to 3 GPa at room temperature (Rigden et al., 1994). Yagi et al. (1992) compressed an end-member $MgSiO_3$ majorite to 10 GPa in the diamond anvil cell at room temperature. Hazen et al. (1994) studied relative compressibilities of several majorite–garnets to ~ 5 GPa. The only high-temperature study was that of Yagi et al. (1987), who measured isothermal compression behavior of synthetic cubic majorite garnets to 10 GPa at 773 K.

In this paper, we report new P–V–T measurements on garnets along the pyrope–majorite join, under pressure and temperature conditions up to 11 GPa and 1173 K, respectively. Complete thermoelastic parameters are extracted from the data on $Py_{62}Mj_{38}$ using various thermal equations of state. These new data, along with our complete equation-of-state analyses on existing data for pyrope, allow us to examine systematics of thermoelastic properties of garnets along the pyrope–majorite join.

2. Experimental

2.1. Specimens

Garnet samples with two compositions along the pyrope–majorite join ($Py_{62}Mj_{38}$ and $Py_{21}Mj_{79}$) were synthesized in a 2000-ton uniaxial split-sphere apparatus (USSA-2000) at the Stony Brook High Pressure Laboratory. Starting materials were glasses with the corresponding compositions and the syntheses were conducted at 18 GPa. Synthesis temperatures were 1473 and 1900 K for $Py_{62}Mj_{38}$ and $Py_{21}Mj_{79}$, respectively, both for 75 min, following a well controlled P–T path in order to produce well-sintered polycrystalline samples with minimal internal stress (Gwanmesia and Liebermann, 1992; see also Rigden et al., 1994). These sintered samples are the most suitable for P–V–T measurements as they generally exhibit no peak broadening when subjected to high pressure (Wang et al., 1997a). Electron microprobe analyses on the samples were published in Parise et al. (1996), who presented high-resolution powder X-ray diffraction data which indicated that the $Py_{62}Mj_{38}$ sample is cubic whereas $Py_{21}Mj_{79}$ is tetragonal; the critical composition for the cubic-tetragonal transition is around $Py_{25}Mj_{75}$.

2.2. P–V–T experiments

P–V–T measurements were carried out in a DIA-6 type cubic-anvil apparatus (SAM-85) at the superconducting beamline (X17B1) of the National Synchrotron Light Source (NSLS) at Brookhaven National Laboratory. Details of the apparatus are described by Weidner et al. (1992). One run (Run #4 in Table 1) was performed in a 6/4 system, in which truncation size of the WC anvils was 4×4 mm^2 and the cubic pressure medium (made of a mixture of amorphous boron and epoxy resin; weight ratio 4:1) was $6 \times 6 \times 6$ mm^3. In later experiments, the straight, 4×4 mm^2 truncation anvils were tapered with an angle of 4° on the anvil flanks, making the final anvil truncations 3.5×3.5 mm^2. Dimensions of the pressure medium remained unchanged. Such a small

Table 1
$P-V-T$ data on majorite garnet ($Py_{62}Mj_{38}$)

P (GPa)	T (K)	V (Å^3)	$\Delta\sigma$	ΔP^a	ΔP^b	ΔP^c
Run #4, n = 25						
5.686	575	1469.9(5)	−0.069	0.067	0.065	−0.056
5.439	778	1477.8(4)	0.043	0.206	0.203	0.233
5.406	875	1486.6(5)	0.003	−0.310	−0.309	−0.268
5.217	969	1489.1(6)	0.009	0.075	0.080	0.113
4.898	776	1483.5(5)	−0.005	0.065	0.063	0.100
4.757	673	1480.6(5)	−0.025	0.053	0.048	0.070
4.595	574	1477.5(5)	0.060	0.126	0.120	0.119
4.445	474	1476.0(7)	0.056	0.014	0.006	−0.017
4.277	374	1472.1(6)	0.051	0.229	0.220	0.182
4.195	301	1470.9(6)	0.047	0.162	0.150	0.122
7.357	978	1471.6(9)	0.021	0.060	0.053	0.058
7.020	772	1466.6(9)	0.017	−0.040	−0.042	−0.029
6.715	571	1461.5(7)	−0.015	−0.045	−0.042	−0.065
6.258	301	1456.2(8)	−0.021	−0.059	−0.058	−0.101
8.297	773	1459.7(8)	−0.064	−0.441	−0.442	−0.440
8.614	971	1463.6(5)	−0.039	−0.237	−0.248	−0.255
8.780	1163	1469.4(7)	−0.010	−0.074	−0.091	−0.157
8.628	1072	1466.9(7)	−0.040	−0.119	−0.134	−0.164
8.471	973	1464.1(6)	−0.032	−0.147	−0.157	−0.164
8.321	872	1460.7(6)	−0.050	−0.094	−0.100	−0.097
8.155	771	1457.6(5)	−0.041	−0.040	−0.040	−0.041
7.947	673	1455.8(6)	−0.020	−0.074	−0.069	−0.084
7.789	573	1453.2(5)	−0.035	−0.042	−0.034	−0.069
7.608	472	1450.6(6)	−0.036	0.032	0.043	−0.014
7.278	302	1447.8(5)	−0.007	0.027	0.036	−0.017
0.000	300	1509.6(5)	0.000	−0.023	−0.055	−0.052
Run #6, n = 57						
0.000	303	1509.1(3)	0.000	0.044	0.012	0.011
10.253	677	1436.7(4)	−0.047	0.213	0.232	0.084
10.130	872	1445.2(2)	−0.023	0.141	0.137	0.112
9.864	1069	1455.6(3)	−0.014	0.072	0.049	0.000
9.388	872	1451.3 3	0.003	0.060	0.054	0.040
9.079	672	1446.8(3)	−0.015	−0.028	−0.018	−0.047
8.785	472	1442.4(2)	−0.022	−0.048	−0.028	−0.098
8.567	307	1439.4(4)	−0.028	−0.100	−0.082	−0.147
8.390	306	1440.2(3)	0.038	−0.038	−0.021	−0.085
7.911	306	1443.0(2)	0.049	0.053	0.067	0.007
9.194	1075	1460.8(2)	0.035	0.108	0.088	0.046
8.809	874	1455.9(3)	0.050	0.051	0.045	0.039
8.439	673	1450.9(3)	0.061	0.072	0.080	0.057
8.112	473	1446.8(2)	0.074	0.033	0.048	−0.015
7.845	307	1443.9(3)	0.089	0.000	0.014	−0.046
8.688	1073	1464.9(2)	0.040	0.079	0.063	0.029
8.305	874	1460.2(2)	0.038	0.001	−0.004	−0.003
7.931	673	1455.3(3)	0.049	0.003	0.008	−0.007
7.575	472	1451.3(2)	0.054	−0.030	−0.020	−0.076
7.295	307	1448.0(3)	0.066	0.002	0.011	−0.044
8.034	1075	1470.5(2)	0.058	0.042	0.030	0.005
7.629	873	1465.5(3)	0.042	−0.009	−0.014	−0.004
7.269	674	1460.9(2)	0.044	−0.050	−0.049	−0.055

Table 1 (continued)

P (GPa)	T (K)	V (Å^3)	$\Delta\sigma$	ΔP^a	ΔP^b	ΔP^c
Run #4, n = 25						
6.925	472	1456.2(3)	0.048	−0.011	−0.004	−0.054
6.663	307	1453.2(2)	0.049	−0.049	−0.046	−0.094
7.231	1074	1476.7(2)	0.020	0.079	0.074	0.059
6.814	873	1471.7(3)	0.062	0.047	0.043	0.063
6.483	672	1467.2(3)	0.080	−0.056	−0.056	−0.053
6.142	473	1462.6(2)	0.078	−0.049	−0.048	−0.088
5.883	307	1459.2(2)	0.061	−0.041	−0.043	−0.084
6.274	1073	1485.0(3)	−0.018	0.048	0.053	0.050
5.830	873	1479.9(3)	0.000	0.035	0.033	0.066
5.468	673	1474.8(3)	0.025	0.037	0.034	0.048
5.153	473	1470.2(2)	0.052	0.002	−0.002	−0.032
4.922	307	1466.9(3)	0.046	−0.049	−0.057	−0.091
5.037	1074	1495.9(3)	0.133	0.045	0.063	0.075
4.587	873	1490.7(3)	0.033	0.030	0.033	0.080
4.221	673	1484.9(3)	0.101	0.090	0.084	0.112
3.882	473	1479.7(3)	0.108	0.131	0.121	0.102
3.681	307	1476.6(3)	0.045	0.012	−0.003	−0.028
4.141	1073	1504.6(3)	−0.040	−0.024	0.006	0.030
2.763	305	1484.4(3)	−0.040	0.006	−0.014	−0.032
4.006	1074	1505.7(3)	−0.030	−0.013	0.019	0.044
3.630	874	1500.3(4)	−0.030	−0.076	−0.067	−0.008
3.376	672	1494.6(4)	−0.109	−0.169	−0.175	−0.136
2.930	471	1488.7(3)	0.037	0.032	0.018	0.008
2.696	306	1485.2(3)	0.029	−0.017	−0.038	−0.055
2.345	305	1488.2(4)	0.053	−0.013	−0.035	−0.050
3.225	1076	1512.6(3)	0.055	0.045	0.087	0.120
2.825	872	1506.9(2)	−0.018	−0.005	0.008	0.075
2.490	673	1500.9(2)	0.016	0.028	0.022	0.068
2.265	473	1495.4(2)	−0.083	−0.038	−0.055	−0.058
2.046	306	1491.0(3)	−0.123	−0.026	−0.050	−0.062
2.149	873	1512.9(4)	0.099	0.045	0.062	0.135
1.753	672	1507.7(4)	0.041	0.028	0.023	0.076
1.450	473	1502.3(3)	0.106	0.021	0.002	0.006
1.241	306	1498.0(3)	0.060	0.010	−0.018	−0.025

$\Delta P = P_{cal} - P_{obs}$, where P_{obs} is the observed pressure (in GPa) and P_{cal} is calculated pressure based on the various equations of state analyzed in this study: [a]high-temperature Birch–Murnaghan, [b]thermal pressure and [c]Mie–Grüneisen–Debye.

change in anvil geometry gained at least 30% pressure capability without sacrificing sample volume, reduced the load-pressure hysteresis to a level within the pressure uncertainty, and improved the survival rate of thermocouple to nearly 100% over a wide range of pressure and temperature conditions (Wang et al., 1997b).

The cell assembly used for all the runs in this

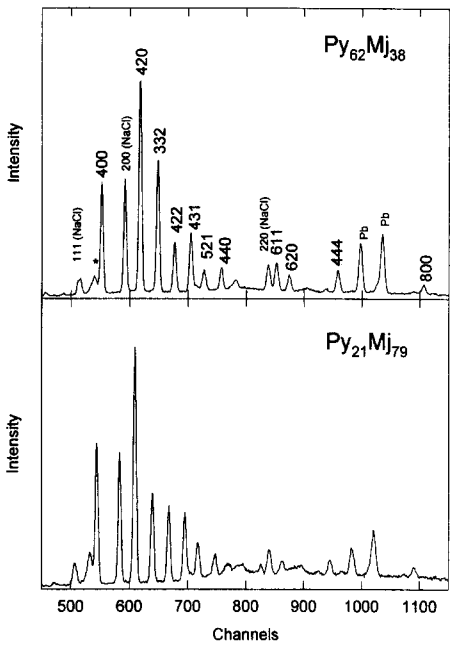

Fig. 1. Examples of the diffraction spectra of $Py_{62}Mj_{38}$ and $Py_{21}Mj_{79}$ obtained at 9.19 GPa, 1075 K and 9.90 GPa, 1067 K, respectively. Peaks from both the sample and the surrounding NaCl pressure medium are labeled for $Py_{62}Mj_{38}$ (they have a one-to-one correspondence in $Py_{21}Mj_{79}$ if indexed as pseudo-cubic). Asterisk indicates peak of BN which is mixed with NaCl; Pb indicates fluorescence peaks of lead. Although peaks for the $Py_{21}Mj_{79}$ sample appear to have comparable widths, most of them are multiplets.

study is described by Wang et al. (1994, 1996). Sintered polycrystalline samples were cut into chunks with linear dimensions of ~ 300 μm and embedded in a mixture of NaCl and BN (weight ratio 4:1), in the center of the sample chamber. The NaCl/BN mixture was dried at 570 K for more than 10 h before the experiment.

The diffraction system was calibrated using the method described by Wang et al. (1994). For the cubic sample $Py_{62}Mj_{38}$, up to 22 peaks were observed with d spacings range from 3.4 to 0.9 Å, 11 of the most intense peaks (non-contaminated) were used for cell refinement. The unit cell volume refinements generally have an uncertainty about 0.3 Å^3 ($\sim \pm 0.02\%$). Examples of the diffraction patterns and unit cell parameter determinations are given in Fig. 1 and Table 2, respectively. For $Py_{21}Mj_{79}$, the tetragonal distortion was too small to be resolved using the current energy-dispersive X-ray technique. Thus, volume data for this sample could only be refined based on a pseudo-cubic index with eight non-overlapped peaks (example also shown in Table 2). Although the refinements gave rather small uncertainties in volume determination, no estimate on real uncertainty could be obtained. This and the change in microstructure after the experiment (discussed in later section) made cell-volume data unreliable and thus cannot be used to extract precise thermoelasticity information.

Table 2
Examples of cell refinement for $Py_{62}Mj_{38}$ and $Py_{21}Mj_{79}$ garnets

$Py_{62}Mj_{38}^a$				$Py_{20}Mj_{80}^b$			
hkl	d_{obs}	d_{cal}	$(d_{cal}-d_{obs})/d_{obs}$	*hkl*	d_{obs}	d_{cal}	$(d_{cal}-d_{obs})/d_{obs}$
400	2.8354	2.8366	0.0001	400	2.8350	2.8327	−0.0002
420	2.5366	2.5372	0.0001	420	2.5333	2.5337	0.0001
332	2.4187	2.4191	0.0001	332	2.4145	2.4158	0.0002
422	2.3162	2.3161	0.0000	422	2.3128	2.3129	0.0000
431	2.2250	2.2252	0.0001	431	2.2216	2.2222	0.0001
611	1.8405	1.8406	0.0000				
620	1.7942	1.7940	−0.0001				
444	1.6379	1.6377	−0.0001				
640	1.5737	1.5735	−0.0001	640	1.5714	1.5713	−0.0001
642	1.5166	1.5162	−0.0002	642	1.5143	1.5142	−0.0001
800	1.4180	1.4183	0.0002				

[a] 9.19 GPa and 1075 K; $a = 11.3465(6)$ Å, $V = 1460.8(2)$ Å^3.
[b] 9.90 GPa and 1067 K; $a = 11.3309(13)$ Å, $V = 1454.8(5)$ Å^3.
Pseudo-cubic index.

As the specimen is in a solid-medium environment, non-hydrostatic stresses are present, which may affect the volume measurement. Weidner et al. (1994) and Wang et al. (1996) have discussed the characteristics of the stress field in SAM-85 and the methods to measure the non-hydrostatic stress [see Fig. 1 of Weidner et al. (1994)]. We determine the macroscopic nonhydrostatic stresses in NaCl by measuring the relative shift of the diffraction lines for NaCl, using the algorithm outlined by Weidner et al. (1994). The macroscopic stress field has a cylindrical symmetry to the first-order approximation, with the vertical stress component σ_1 differs from horizontal $\sigma_2 \approx \sigma_3$ [see Fig. 1 of Weidner et al. (1994)]. Under such a stress condition, each diffraction peak *hkl* [representing the spacing of the (*hkl*) lattice planes] is shifted from the hydrostatic condition by an amount that is proportional to the elastic compliance of the crystal along that crystallographic orientation. By observing *d*-spacings of several non-parallel lattice planes in NaCl, differential stress $(\sigma_1 - \sigma_3)$ can be calculated. The measured $(\sigma_1 - \sigma_3)$ values represent approximately the differential stress boundary condition on the sample, which is embedded in NaCl [see Fig. 1 of Weidner et al. (1994)]. Each volume measurement is thus associated with three parameters: pressure, temperature and differential stress, $(\sigma_1 - \sigma_3)$. At room temperature, the magnitude of the non-hydrostatic stress can amount to as much as 0.3 GPa. The most efficient way to minimize non-hydrostatic stress is heating, as the strengths of NaCl and BN decrease dramatically with increasing temperature (Weidner et al., 1994). Above 600 K or immediately after cooling from above this temperature the measured non-hydrostatic stress is generally below 0.1 GPa, which is about the detectability of the current technique. Thus, *P–V–T* measurements were carried out only during and after heating to 1100 K.

Pressure–temperature paths for the experiments are similar for all the runs. The sample was compressed at room temperature to the maximum pressure and then heated to the maximum temperature in order to release non-hydrostatic stress caused by the finite strength of the BN/NaCl pressure medium. Data collection was carried out at several fixed temperatures under constant ram load. Pressure was then decreased at room temperature and the sample

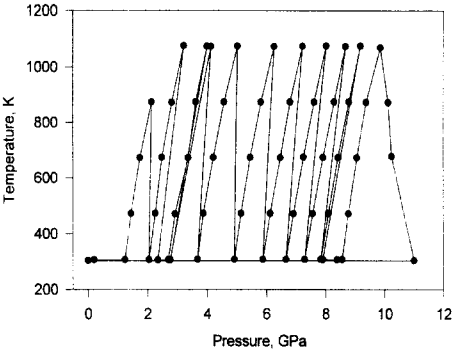

Fig. 2. Pressure–temperature path of run #6. Ram load is increased first at room temperature to reach the maximum pressure (~ 11 GPa), then temperature is increased to a maximum of 1073 K with ram load remained fixed. An apparent pressure drop can be seen which is partly due to reduction of nonhydrostatic stress. Still at the fixed ram load, *P–V–T* data are obtained on decreasing temperature. The further decrease in pressure (to about 8.5 GPa at room temperature) is due to the loss in thermal pressure. At room temperature, ram load is then decreased to just below 8 GPa. Heating increases the pressure because the thermal pressure is now recovered. Each point represents the condition where the unit-cell volume of the sample is taken.

heated again to the peak temperature, followed by data collection at the fixed temperature points. The procedure was repeated for up to 11 temperature excursions to create a uniform *P,T* grid for volume measurements. Fig. 2 shows one such *P–T* path. At each *P,T* point, an energy dispersive X-ray spectrum was collected for both the sample and the pressure medium immediately adjacent to the sample (about 200 μm apart). Pressure was determined by thermal equation of state of NaCl (Decker, 1971) and temperature was measured with a W/Re26%–W/Re5% thermocouple.

3. Results

3.1. Reversibility

As the runs were conducted at pressure conditions outside the thermodynamic stability field of the garnets, samples recovered after the *P–V–T* measurements were examined by transmission electron microscopy (TEM), in order to detect any irreversible change that may occur during the experiments. No sign of alternation in structure and microstructure was observed in the $Py_{62}Mj_{38}$ sample.

The $Py_{21}Mj_{79}$ sample also remained tetragonal after the run; however, TEM revealed that microtwin domains in the sample have been coarsened (compare Fig. 3A and B), suggesting that varying degrees of relaxation in stress field may have taken place across the domain walls during the experiment. Wang et al. (1993) studied the end member majorite $MgSiO_3$ quenched from various temperatures using TEM and observed a clear sequence of coarsening in microdomains from a fine, 'tweed' structure to submicron twin domains. They concluded that a phase transition may have occurred around 2620 K at 22 GPa. The same cubic-tetragonal transition also occurs as a function of composition. Parise et al. (1996) studied samples quenched from 1900 K along the pyrope–majorite join by high-resolution synchrotron powder X-ray diffraction and concluded, based on systematic absences and peak shape, that a cubic-tetragonal transition occurs at a composition about $Py_{25}Mj_{75}$ (see Table 3). In a study using conventional powder X-ray diffraction, Heinemann et al. (1996) placed the transition at $Py_{20}Mj_{80}$, based

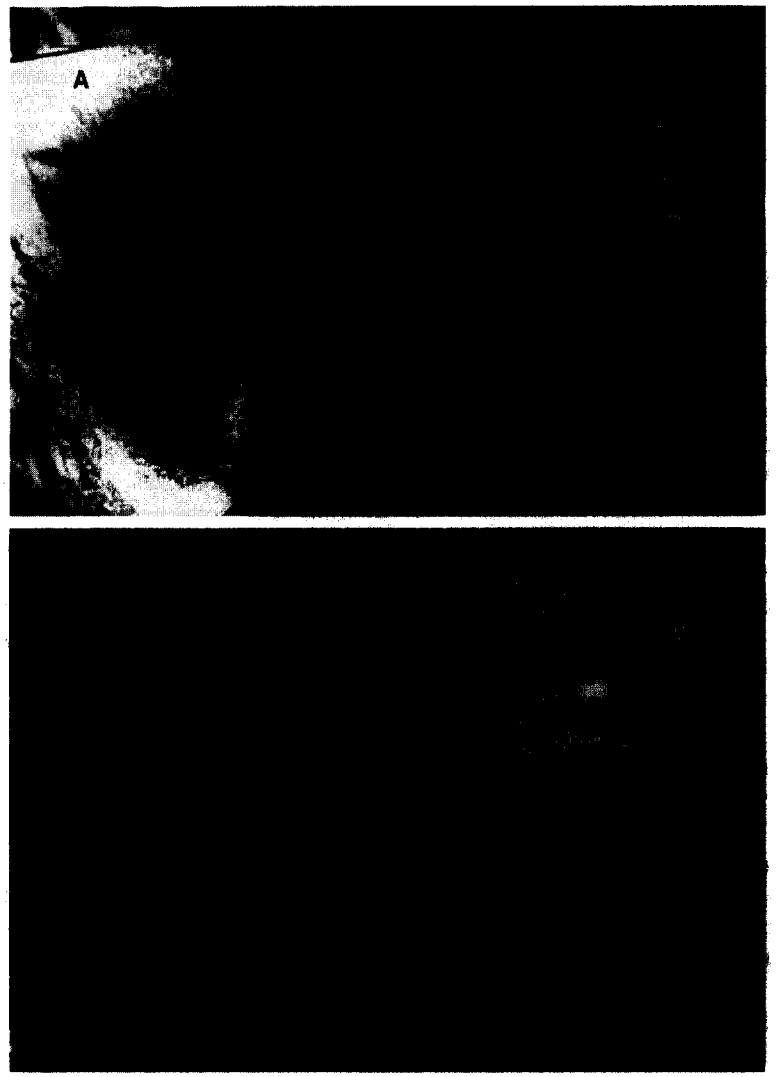

Fig. 3. Microstructure of the tetragonal garnet $Py_{21}Mj_{79}$ before (A) and after (B) the P–V–T experiment. A coarsening in twin-domain structure is clearly seen (note difference scales).

Table 3
Zero-pressure cell parameters of garnets along the pyrope–majorite join

Composition	a (Å)	c (Å)	V (Å^3)	References
Py_{100}	11.455(3)	–	1503.1(11)	Yagi et al. (1987)
Py_{100}	11.452(1)	–	1501.9(1)	Parise et al. (1996)
$Py_{62}Mj_{38}$	11.468(1)	–	1508.2(2)	Parise et al. (1996)
$Py_{62}Mj_{38}$	11.4702(8)	–	1509.1(3)	This study
$Py_{52}Mj_{48}$	11.4735(5)	–	1510.4(2)	Parise et al. (1996)
$Py_{50}Mj_{50}$	11.472(3)	–	1509.7(10)	Sinogeikin et al. (1996)
$Py_{42}Mj_{58}$	11.474(3)	–	1510.6(11)	Yagi et al. (1987)
$Py_{25}Mj_{75}$	11.4783(3)[a]	–	1512.3 (2)[a]	Parise et al. (1996)
$Py_{21}Mj_{79}$	11.494(1)	11.457(1)	1513.6(2)	Parise et al. (1996)
$Py_{20}Mj_{80}$	11.482(3)[a]	–	1513.8(10)[a]	Sinogeikin et al. (1996)
Mj_{100}	11.491	11.406	1506.1	Kato and Kumazawa (1985)
Mj_{100}	11.501	11.480	1518.5	Angel et al. (1989)
Mj_{100}	11.516	11.428	1515.6	Matsubara et al. (1990)
Mj_{100}	11.509	11.423	1513.1	Yagi et al. (1992)
Mj_{100}	11.500(4)	11.445(5)	1513.6(15)	Sinogeikin et al. (1996)
Mj_{100}	11.514(1)	11.423(1)	1514.3(3)	Pacalo and Weidner (1996)

[a]Assumed cubic.

on peak shape and cell parameter determination. These latter authors observed pervasive twinning in all the tetragonal garnets quenched from 18–19 GPa and 2170–2270 K, and proposed that all of the garnets were in fact cubic under synthesis conditions and that twin domains in the tetragonal garnets were due to cubic-tetragonal phase transition upon quenching. If this is indeed the case, ordering of Si and Mg atoms on the octahedral site must take place in a few seconds during quenching, implying unrealistically fast diffusion rates for Mg and Si. The conclusion is significantly weakened, however, by the fact that their synthesis conditions were characterized by very short heating duration (maximum 15 min) and that the samples were often mixed with low-pressure phases, suggesting that equilibrium had not been reached.

The cubic-tetragonal transition could depend strongly on composition, as suggested by the change in spontaneous strain in the tetragonal phases. Thus, the microtwins in the $Py_{21}Mj_{79}$ sample could be due to either a phase transition during synthesis or on a decrease of pressure and temperature, resulting in high internal stress in the sintered sample. As the domains were coarsened during the P–V–T experiment, stress field across the domains may have been altered. Indeed, unit cell volumes measured at ambient conditions before ($\sim$ 1509 Å^3) and after ($\sim$ 1514 Å^3) the P–V–T run differed by 0.3%. This difference is a factor of 5 greater than the estimated uncertainties (0.05 Å^3) in volume measurement. The irreversible change in microstructure and the fact that the tetragonal distortion could not be resolved in cell volume refinement are two important factors that may bias the experimental results. Data for this sample are therefore excluded in equation-of-state analysis.

3.2. Room-temperature compression and bulk modulus

P–V–T data are summarized in Table 1; only the 'hydrostatic' points are included, whose non-hydrostatic stress ($\Delta\sigma$) levels are generally below 0.1 GPa. Pressure misfits in various equation-of-state analyses are also presented in order to compare the extracted thermoelastic properties.

The ambient volumes for $Py_{62}Mj_{38}$ before and after the P–V–T runs are consistent with each other and with previous measurements. Fig. 4 shows the room-temperature volume data after stress annealing. These data are fit by the third-order Birch–Murnaghan equation of state

$$P = 3/2\,K_{T0}\left[\eta^{7/3} - \eta^{5/3}\right]\left[1 + 3/4\left(K'_{T0} - 4\right) \times \left(\eta^{2/3} - 1\right)\right], \quad (1)$$

where K_{T0} and K'_{T0} are the ambient isothermal bulk modulus and its pressure derivative, respectively, and $\eta = V_0/V$. For data from run #6 alone, the results with a weighted least-squares fit are $V_0 =$ 1509.1(3) Å^3, $K_{T0} = 162.1(13)$ GPa, and $K'_{T0} =$ 4.4(4). If K'_{T0} is chosen to be 5.3 (the pressure derivative of the adiabatic bulk modulus as measured by Rigden et al., 1994), then $V_0 = 1509.1(3)$ Å^3 and $K_{T0} = 159.8(13)$ GPa. An unweighted fit to the combined data set from both runs #4 and #6 yields $V_0 = 1509.4(3)$ Å^3, $K_{T0} = 159(3)$ GPa, and $K'_{T0} =$ 5.0(8), to compare with the ultrasonic data on a specimen with the same composition (Rigden et al., 1994): $K_{S0} = 168.5(6)$ GPa and $K'_{S0} = 5.3(2)$. The unweighted fit is shown by the solid curve in Fig. 4.

Fig. 5 compares our K_{T0} values for $Py_{62}Mj_{38}$ with previous results on garnets along the pyrope–majorite join using both static compression and wave-propagation techniques such as Brillouin spectroscopy and ultrasonics (in which cases the bulk moduli are adiabatic). For an ambient Grüneisen parameter of $\gamma_0 = 1.3$ and thermal expansion of $\alpha_0 = 2.5 \times 10^{-5}$ K^{-1}, the difference between K_T and K_S is about 1%, smaller than the estimated errors in most of the measurements. Large scatter is evident in these data; any systematic trend, if exists, is a very slight decrease in K_{T0} with increasing majorite content. Sinogeikin et al. (1996) proposed a break in the trend, with K_{T0} remaining constant between Py_{100} and $Py_{20}Mj_{80}$, followed by a lower, but again constant K_{T0}. Although there is now evidence for a structural phase transition across $Py_{25}Mj_{75}$ (Parise et al., 1996), existing ambient bulk modulus data indicate that any change, if exists, would be small and therefore a continuous, linear relation may be appropriate to describe the trend (Yeganeh-Haeri et al., 1990; Pacalo and Weidner, 1996; Sinogeikin et al., 1996). Yagi et al. (1992) and Sinogeikin et al. (1996) proposed composition dependence in bulk moduli, in terms of majorite content (X_{Mj}), to be K_{T0} (GPa) = 171.8(35) − 0.11(50) X_{Mj} (where K'_{T0} is assumed to be 4) and K_{S0} (GPa) = 173 − 0.1 X_{Mj}, respectively. According to the former relation, the predicted K_{T0} for $Py_{62}Mj_{38}$ would be 165(6) GPa. This is somewhat higher than what we have measured but in general agreement considering the uncertainties, especially considering the lower K'_{T0} values used by Yagi et al. (1992) in obtaining the K_{T0} values.

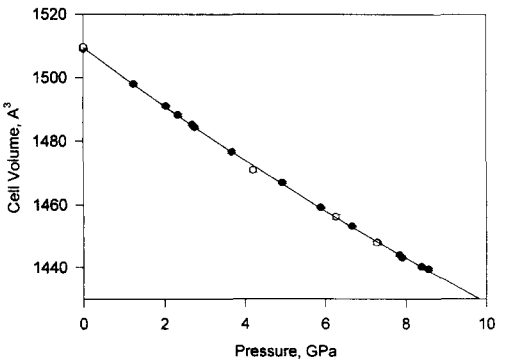

Fig. 4. Room-temperature compression data of majorite garnet $Py_{62}Mj_{38}$. Solid circles data from run #6; open circles from #4. Solid curve the fit using the Birch–Murnaghan equation of state. Error bars are smaller than the size of the symbols.

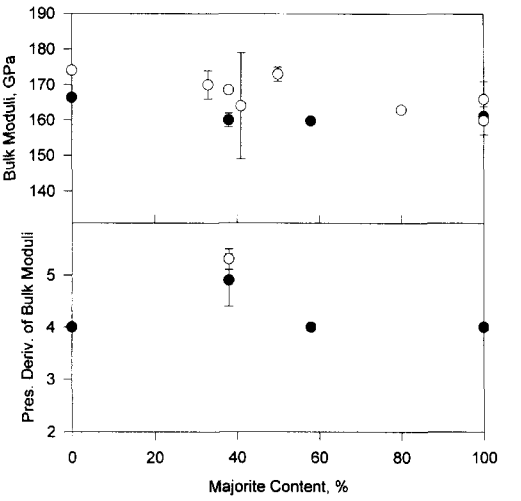

Fig. 5. Comparison of bulk moduli and their pressure derivatives on garnets along the pyrope–majorite join. Open symbols represent adiabatic properties measured with Brillouin scattering (B) and ultrasonic (U) techniques, solid symbols isothermal properties from $P-V-T$ measurements (V). In the lower panel, all of the $K'_{T0} = 4$ points are assumed values in the Birch–Murnaghan equation-of-state fit. Sources of data: pyrope: Leitner et al. (1980) (B), Yagi et al. (1987)(V); $Py_{67}Mj_{33}$: Yeganeh-Haeri et al. (1990) (B); $Py_{62}Mj_{38}$: Rigden et al. (1994) (U), this study (V); $Py_{59}Mj_{41}$: Bass and Kanzaki (1990) (B); $Py_{50}Mj_{50}$: Sinogeikin et al. (1996) (B); $Py_{42}Mj_{58}$: Yagi et al. (1987) (V); $Py_{79}Mj_{21}$: Sinogeikin et al. (1996) (B); majorite Mj_{100}: Sinogeikin et al. (1996) (B); Pacalo and Weidner (1996) (B); Yagi et al. (1992) (V).

3.3. Thermal equation of state analysis

3.3.1. High-temperature Birch–Murnaghan equation of state

Fig. 6 shows the volume data measured at various pressure and temperature conditions. We first analyze the data with a high-temperature Birch–Murnaghan (HTBM) equation of state, which is described again by Eq. (1), except now $\eta = V_R/V$, and K_{T0}, V_R, and K'_{T0} are all parameters at zero pressure and at a constant temperature T. $V_R = V(0,T)$ is related to V_0 via zero-pressure thermal expansion $\alpha(0,T)$,

$$V_R = V_0 \exp\left[\int \alpha(0,T)\mathrm{d}T\right].$$

In this expression the integral is from 300 K to T and

$$\alpha(0,T) = a + bT - cT^{-2}, \qquad (2)$$

where a, b and c are positive constants. K'_{T0} is again assumed constant (= 5 for our sample). Only first-order derivatives of K_T are considered in all of the fits presented below.

An unweighted least-squares fit to the combined data set from both runs yields $K_{T0} = 159(2)$ GPa, $K'_{T0} = 4.9(6)$, $a = 2.08(14) \times 10^{-5}$ K^{-1}, $b = 1.43(21) \times 10^{-8}$ K^{-2}, and $(\alpha K_T/\alpha T)_P = 0.019(4)$ GPa K^{-1}. The coefficient c in the zero pressure thermal expansion cannot be resolved even when both K_{T0} and K'_{T0} are fixed and is thus set to zero in the fit. The fit is shown in Fig. 6 and the misfits in pressures are given in Table 1.

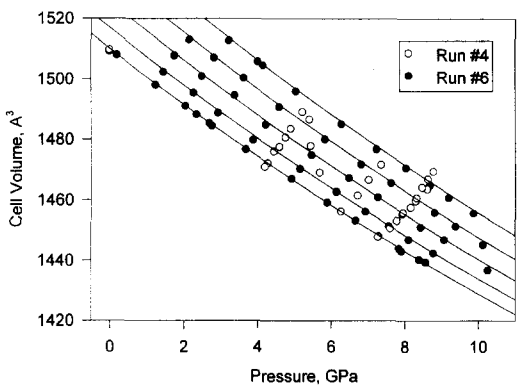

Fig. 6. P–V–T data of $Py_{62}Mj_{38}$ garnet with the HTBM fits. Solid circles data from run #6, open circles from run #4. Solid curves are isothermal fits at various temperatures (from lower volumes), 300, 473, 673, 873 and 1073 K, respectively.

3.3.2. Thermal pressure equation of state

We also analyze the data using the thermal-pressure equation-of-state (Anderson, 1984, 1996, Anderson et al., 1989). This approach is based on the Mie–Grüneisen theory, by computing thermal pressures with respect to the room-temperature equation of state. At any temperature T and for a given volume V, the pressure is expressed as the sum of the static pressure at room temperature T_0 and the thermal pressure ΔP_{th} (e.g., see Jackson and Rigden, 1996):

$$P(V,T) = P(V,T_0) + \Delta P_{th} = \Sigma b_i X_i(\eta,T) \qquad (3a)$$

where

$$\begin{aligned} X_1 &= \eta^{7/3} - \eta^{5/3} & b_1 &= 3K_T(V_0,T_0)/2 \\ X_2 &= X_1(\eta^{2/3} - 1) & b_2 &= 9/8 K_T(V_0,T_0) \\ & & & [K'_{T0}(V_0,T_0) - 4] \\ X_3 &= (T - T_0), & b_3 &= \alpha K_T \\ X_4 &= -(T - T_0)\ln\eta & b_4 &= (\partial K_T/\partial T)_V \\ X_5 &= (T - T_0)^2 & b_5 &= \left[(\partial^2 P/\partial T^2)_V\right]/2. \end{aligned} \qquad (3b)$$

The 'static' pressure and thermal pressure are respectively given by

$$P_s(V,T_0) = b_1 X_1 + b_2 X_2 \qquad (4a)$$

and

$$\Delta P_{th}(V,T) = b_3 X_3 + b_4 X_4 + b_5 X_5 \qquad (4b)$$

An unweighted fit to the data from both runs #4 and #6 using Eqs. (3a) and (3b) with all five terms (but again with a fixed $K'_{T0} = 5$) yields $V_0 = 1509.1(3)$ Å^3, $K_{T0} = 158.1(12)$ GPa, and $\alpha_0 = 2.50(10) \times 10^{-5}$ K^{-1}. The coefficient b_4 is found to be in the order of -2×10^{-3} GPa K^{-1}, with an uncertainty about twice the magnitude; clearly b_4 cannot be resolved from this fit. When b_4 is fixed at 0, we obtain $V_0 = 1509.1(3)$ Å^3, $K_{T0} = 159(1)$ GPa, $\alpha_0 = 2.53(9) \times 10^{-5}$ K^{-1}, and $b_5 = 9.3(18) \times 10^{-7}$ GPa^{-2} K^{-2}, with no significant change in the variance. From the well-known thermodynamic identity $(\partial K_T/\partial T)_V = (\partial K_T/\partial T)_P + \alpha K_T(\partial K_T/\partial P)_T$, we ob-

tain, at ambient condition, $(\partial K_T/\partial T)_P = -\alpha_0 K_{T0} K'_{T0} = -0.020(2)$ GPa K^{-1}. The fit is shown in Fig. 7, in the form of thermal pressure. The pressure misfits are again given in Table 1.

The fact that as $b_4 = (\partial K_T/\partial T)_V = 0$ indicates that thermal pressure is independent of volume and therefore $\Delta P_{th}(V,T) = \Delta P_{th}(V_0,T)$. This is better illustrated in Fig. 8, where thermal pressures remain essentially constant over a wide range of volume and temperature. Thus, the thermal-pressure equation of state consists of two separate functions: static pressure that is a function of volume only and thermal pressure which is a function of temperature only. A number of silicates exhibit this property over the experimental P–T range, including $(Mg,Fe)_2SiO_4$ olivine (Anderson et al., 1992; Guyot et al., 1996), $CaSiO_3$ perovskite (Wang et al., 1996), and garnet (this study). As pointed out by Anderson et al. (1992), this implies that the Anderson–Grüneisen parameter $\delta_T \equiv -(\partial K_T/\partial T)_T/(\alpha K_T) = K'_T$ over the entire P–T range of our experiment.

3.3.3. A lattice dynamic equation of state based on the Mie–Grüneisen–Debye model

Jackson and Rigden (1996) proposed a Mie–Grüneisen–Debye (MGD) equation of state in which the Mie–Grüneisen equation of state is used, whereby the thermal energy is approximated by the well-known Debye lattice virational model, with only the acoustic modes taken into account. We have also fitted our data in this equation of state. In all of the fits, Debye temperature θ_D is chosen as 730 K,

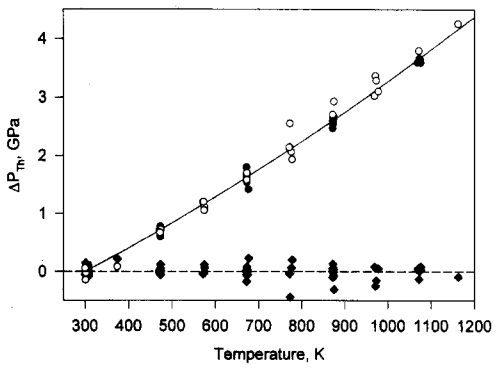

Fig. 7. Thermal-pressure equation-of-state fit. Solid circles data from run #6, open circles from run #4. Diamonds represent misfit in thermal pressure.

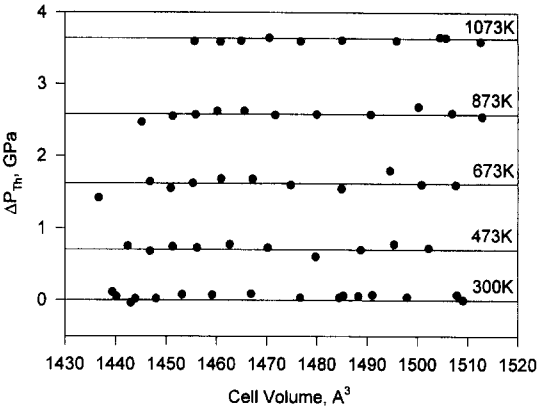

Fig. 8. Thermal pressure measured in Run #6 plotted against cell volume at various temperatures. Clearly, thermal pressure is virtually independent of volume. Horizontal solid lines are guide to the eye.

based on acoustic velocity measurements on a polycrystalline sample with the same composition (Rigden et al., 1994). The volume dependence of the Grüneisen parameter γ on volume is expressed as $\gamma/\gamma_0 = (V/V_0)^q$, where we assume $q = 1$. Jackson and Rigden (1996) have shown that in this approach the results are generally insensitive to the choice of θ_D and q. Indeed, when θ_D is varied by ± 100 K, the results still agree within the error bars, and the RMS misfit pressure level remains unchanged.

Table 4 lists the results of unweighted fit to the $Py_{62}Mj_{38}$ garnet, as well as the RMS misfits in pressure. In Table 1, the pressure misfit for each data

Table 4
Thermoelastic properties of Py_XMj_{1-X} garnets from the MGD equation of state

Properties	Py_{100}	$Py_{62}Mj_{38}$
V_0 (Å^3)	1503.1(5)	1509.1(3)
θ_D (K)	[790][a]	[730][a]
γ_0	1.17(2)	1.17(1)
K_{T0} (GPa)	171(4)	158(4)
α_0, 10^{-5} K^{-1}	2.2(2)	2.5(2)
K'_{T0}	[5.0][a]	4.9(1)
$(\partial K_T/\partial T)_V$ (GPa K^{-1})	−0.0027(5)	−0.0024(5)
$(\partial K_T/\partial T)_P$ (GPa K^{-1})	−0.021(2)	−0.022(1)
$(\partial\alpha/\partial T)_V$ (10^{-8} K^{-2})	4.5(13)	4.4(14)
$(\partial\alpha/\partial T)_P$ (10^{-8} K^{-2})	4.8(13)	4.7(14)
RMS misfit (GPa)	0.148	0.103

[a]Assumed and fixed values.

point is also presented so that the results can be compared to the fits using other equations of state presented in previous sections.

4. Discussion

4.1. Thermal equation of state of Py_{100} from existing data

Pyrope has been studied previously by a number of authors. The zero-pressure thermal expansion behavior was measured by Skinner (1956) and Ohsako (as cited in Yagi et al., 1987). Suzuki and Anderson (1983) studied a natural garnet close to the pure pyrope composition. Yagi et al. (1987) measured P–V–T relation of Py_{100} at high pressure and temperature, using a DIA-type, cubic-anvil apparatus (MAX-80); they corrected the slight pressure changes at various temperatures (between 800 and 1300 K) and published an isobaric data set at 6 GPa.

Yagi et al. (1987) analyzed these data and expressed the volume data of Skinner (1956) and Ohsako by a second-order polynomial function of temperature to obtain thermal expansivity of pyrope at zero pressure and 6 GPa. Here, we combine these data and fit the entire data set using the three equations of state described above, in order to obtain a consistent thermoelastic parameter set and examine the systematics of the thermoelasticity of garnets along the pyrope–majorite join.

For the HTBM equation of state, fixing $K'_{T0} = 5$ yields $K_{T0} = 170(2)$ GPa and $(\partial K_T/\partial T)_P = -0.020(3)$ GPa K^{-1}. The zero-pressure thermal expansion is found to be $\alpha(\text{in } K^{-1}) = 2.28(19) \times 10^{-5} + 9.42(282) \times 10^{-9}\ T$ (see Table 5). The third term [i.e., coefficient c in Eq. (2)] cannot be resolved. This expression gives an average thermal expansion of 3.0×10^{-5} K^{-1}, between 300 and 1200 K, identical to that measured by Suzuki and Anderson (1983).

For the thermal-pressure equation of state, the coefficient b_4 is found to be non-resolvable from zero, similar to the case of $Py_{62}Mj_{38}$. When K'_{T0} is fixed at 5 and b_4 at zero, we obtain $K_{T0} = 171(1)$ GPa, $\alpha_0 = 2.56(10) \times 10^{-5}$ K^{-1}, and $2b_5 = (\partial^2 P/\partial T^2)_V = 1.0(5) \times 10^{-6}$ GPa^{-2} K^{-2}. These parameters remain essentially unchanged when K'_{T0} is varied from 4.0 to 5.0. The corresponding $(\partial K_T/\partial T)_P$ is $-0.019(2)$ GPa K^{-1}.

Table 5
Thermoclastic parameters of garnets using the HTBM equation of state

Parameters	Py_{100}	$Py_{62}Mj_{38}$
V_0 (Å^3)	1503.1(5)	1509.1(3)
K_{T0} (GPa)	170(2)	159(2)
K'_{T0}	[5][a]	4.9(6)
$\alpha_0 = a + bT - cT^{-2}$		
a (10^{-5} K^{-1})	2.3(2)	2.1(1)
b (10^{-8} K^{-2})	0.94(28)	1.4(2)
c (K)	0.0	0.0
$(\partial K_T/\partial T)_P$ (GPa K^{-1})	−0.020(3)	−0.019(4)

[a]Assumed value.

The MGD equation of state yields similar results which are listed in Table 4. Overall, temperature related properties [$(\partial K_T/\partial T)_P$, $(\partial K_T/\partial T)_V$, and α] of pyrope are virtually indistinguishable from those of $Py_{62}Mj_{38}$.

4.2. Systematics in thermoelastic properties for garnets along the pyrope–majorite join

There is accumulating evidence for a structural phase transition in majorite garnets. With increasing pyrope content, the tetragonal majorite transforms to cubic at around 75 mol% majorite (Parise et al., 1996). TEM observation on microstructure of end member majorite ($MgSiO_3$) samples quenched from various temperatures suggests that a cubic-tetragonal phase transition occurs around 2620 K (Wang et al., 1993). All these data suggest that the cubic-tetragonal phase transition along the majorite–pyrope join is sensitive to both composition and temperature. Ambient elasticity data show little deviation form a linear, continuous trend as a function of composition (Yagi et al., 1987; Yeganeh-Haeri et al., 1990; Pacalo and Weidner, 1996; Sinogeikin et al., 1996). The question of whether the phase transition affects temperature derivatives of the elastic constants in any significant way has important implications in modeling the mineralogy of the transition zone.

Our data provide a direct assessment of temperature derivatives of the bulk modulus of garnets as a function of majorite content. Various equation-of-state fits to the data for $Py_{62}Mj_{38}$ and pyrope yield

remarkably consistent thermoelastic properties. Therefore, we conclude that there is no significant anomalous behavior with increasing majorite content as long as the garnet structure remains cubic. Preliminary analysis on the data for $Py_{21}Mj_{79}$ garnet also suggests that bulk modulus and density of the tetragonal garnets behave rather similarly to the cubic counterparts. However, the pseudo-cubic approximation in measuring the tetragonal cell volume and stress relaxation due to domain coarsening in the majorite-rich sample during the measurement prevent us from drawing definitive conclusions. Higher-resolution studies are needed.

5. Conclusions

Using synchrotron X-radiation and a DIA-type, cubic anvil apparatus, P–V–T measurements on garnets along the majorite–pyrope join have been carried out at pressures between 0 and 11 GPa and temperatures up to 1170 K, under quasi-hydrostatic conditions with non-hydrostatic stresses carefully determined. A complete thermal equation of state has been determined for $Py_{62}Mj_{38}$. Three equations of state gave remarkably consistent thermoelastic properties. Notably, thermal pressure is independent of volume over a wide temperature (up to 1170 K) and compression range (up to 5%).

Previous data on pyrope are combined and reanalyzed using the same approach. Comparison with Py_{100} and $Py_{62}Mj_{38}$ indicates that most temperature related properties $[(\partial K_T/\partial T)_P$, $(\partial K_T/\partial T)_V$, and $\alpha]$ are insensitive to majorite content in garnet between Py_{100} and $Py_{62}Mj_{38}$.

Our data on the $Py_{21}Mj_{79}$ garnet are likely to have been affected by several factors, including insufficient resolution for the tetragonal distortion and stress relaxation in the polycrystalline sample due to domain coarsening. Although preliminary analysis showed no convincing break in the thermoelastic properties in all pyrope–majorite solid–solution garnets, definitive answers await for further studies.

With previous measurements on the high pressure polymorphs of olivine (Fei et al., 1992a; Meng et al., 1993, 1994) and $CaSiO_3$ perovskite (Wang et al., 1996), these new data on majorite garnets allow quantitative analyses on composition of the Transition Zone. Applications of the data will be dealt with in a separate paper.

Acknowledgements

We wish to thank M.T. Vaughan, I. Martinez, and Y. Sinelnikov for their assistance during the experiments. We also thank D. Chapman, N. Lazarz, and W. Thomlinson of the X17 beamline at NSLS for their technical assistance. We are especially grateful to Ian Jackson, who provided the program for the MGD equation-of-state analyses. We thank two reviewers for comments. The SAM-85 project was supported by the NSF grant for the Center for High Pressure Research (CHiPR), EAR89-20239. This work was partially supported by the NSF grants EAR95-26634 and 93-04502, MPI contribution No. 206.

References

Akaogi, M., Akimoto, S., 1977. Pyroxene–garnet solid–solution equilibria in the system $Mg_4Si_4O_{12}$–$Mg_3Al_2Si_3O_{12}$ and $Fe_4Si_4O_{12}$–$Fe_3Al_2Si_3O_{12}$ at high pressures and temperatures. Phys. Earth Planet. Int. 15, 90–106.

Anderson, O.L., 1984. A universal equation of state. J. Geodyn. 1, 185–214.

Anderson, O.L., 1996. The volume dependence of thermal pressure in insulator solids, Eos. Trans. Am. Geophys. Union 77, F747suppl.

Anderson, O.L., Isaak, D.G., Yamamoto, S., 1989. Anharmonicity and the equation of state of gold. J. Appl. Phys. 65, 1534–1543.

Anderson, O.L., Isaak, D.G., Oda, H., 1992. High-temperature elastic constant data on minerals relevant to geophysics. Rev. Geophys. 30, 57–90.

Angel, R.J., Finger, L.W., Hazen, R.M., Kanzaki, M., Weidner, D.J., Liebermann, R.C., Veblen, D.R., 1989. Structure and twinning of single-crystal $MgSiO_3$ garnet synthesized at 17 GPa and 1800°C. Am. Mineral. 74, 509–512.

Bass, J.D., Kanzaki, M., 1990. Elasticity of majorite–pyrope solid solution. Geophys. Res. Lett. 17, 1989–1992.

Decker, D.L., 1971. High-pressure equation of state for NaCl, KCl, and CsCL. J. Appl. Phys. 42, 3239–3244.

Fei, Y., Mao, H.-K., Shu, J., Parthasarathy, G., Bassett, W.A., Ko, J., 1992a. Simultaneous high-p. high-T X-ray diffraction study of β-$(Mg,Fe)_2SiO_4$ to 26 GPa and 900 K. J. Geophys. Res. 97, 4489–4495.

Gasparik, T., 1989. Transformation of enstatite–diopside–jadeite pyroxenes to garnet. Contrib. Mineral. Petrol. 102, 389–405.

Gasparik, T., 1990. Phase relations in the transition zone. J. Geophys. Res. 95, 15751–15769.

Gasparik, T., 1996. Melting experiments on the enstatite–diopside join at 70–224 kbar, including the melting of diopside. Contrib. Mineral. Petrol. 123.

Gwanmesia, G.D., Liebermann, R.C., 1992. Polycrystals of high-pressure phases of mantle minerals: hot-pressing and characterization of physical properties. In: Syono, Y., Manghnani, M.H. (Eds.), High Pressure Research: Application of Earth and Planetary Sciences. Terrapub, Tokyo–Am. Geophys. Union, Washington, DC, pp. 117–135.

Guyot, F., Wang, Y., Gillet, Ph., Ricard, J., 1996. Quasi-harmonic computations of thermodynamic parameters of olivines at high pressure and high temperature: A comparison with experimental data. Phys. Earth Planet. Int. 98, 17–29.

Hazen, R.M., Downs, R.T., Conrad, P.G., Finger, L.W., Gasparik, T., 1994. Comparative compressibilities of majorite-type garnets. Phys. Chem. Minerals 21, 344–349.

Heinemann, S., Sharp, T.G., Seifert, F., Rubie, D.C., 1996. The cubic-tetragonal phase transition in the system majorite ($Mg_4Si_4O_{12}$)–pyrope ($Mg_3Al_2Si_3O_{12}$), and garnet symmetry in the Earth's transition zone, Phys. Earth Planet. Int., in press.

Jackson, I., Rigden, S.M., 1996. Analysis of $P-V-T$ data: constraints on the thermoelastic properties of high-pressure minerals. Phys. Earth Planet. Int. 96, 85–112.

Kato, T., Kumazawa, M., 1985. Garnet phase of $MgSiO_3$ filling the pyroxene–ilmenite gap at very high temperature. Nature 316, 803–805.

Kanzaki, M., 1987. Ultra high-pressure phase relations in the system $MgSiO_3$–$Mg_3Al_2Si_3O_{12}$. Phys. Earth Planet. Int. 49, 168–175.

Leitner, L., Weidner, D.J., Liebermann, R.C., 1980. Elasticity of single crystal pyrope and implications for garnet solid solution senes. Phys. Earth Planet. Int. 22, 111–121.

Matsubara, R., Toraya, H., Tanaka, S., Sawamoto, H., 1990. Precision lattice-parameter determination of (Mg,Fe)SiO_3 tetragonal garnets. Science 247, 697–699.

Meng, Y., Weidner, D.J., Gwamnesia, G.D., Liebermann, R.C., Vaughan, M.T., Wang, Y., Leinenweber, K., Pacalo, R.E., Yeganeh-Haeri, A., Zhao, Y., 1993. In situ high $P-T$ X-ray diffraction studies on three polymorphs (α, β, γ) of Mg_2SiO_4. J. Geophys. Res. 98, 22199–22207.

Meng, Y., Fei, Y., Weidner, D.J., Gwamnesia, G.D., Hu, J., 1994. Hydrostatic compression of γ-Mg_2SiO_4 to mantle pressures at 700 K: Thermal equation of state and related thermoelastic properties. Phys. Chem. Minerals 21, 407–412.

Pacalo, R.E.G., Weidner, D.J., 1996. Elasticity of majorite, $MgSiO_3$ tetragonal garnet. Phys. Earth Planet. Int. 99, 145–154.

Parise, J.B., Wang, Y., Gwanmesia, G.D., Zhang, J., Sinelnikov, Y., Chmielowski, J., Weidner, D.J., Liebermann, R.C., 1996. The symmetry of garnets on the pyrope ($Mg_3Al_2Si_3O_{12}$)–majorite ($MgSiO_3$) join. Geophys. Res. Lett. 23, 3782–3799.

Rigden, S.M., Gwanrnesia, G.D., Liebermann, R.C., 1994. Elastic wave velocities of a pyrope–majorite garnet to 3 GPa. Phys. Earth Planet. Int. 86, 35–44.

Sinogeikin, S.V., Bass, J.D., O'Neill, B., Gasparik, T., 1996. Elasticity of tetragonal end member majorite and solid solutions in the system $Mg_4Si_4O_{12}$–$Mg_3Al_2Si_3O_{12}$. Phys. Earth Planet. Int., in press.

Skinner, B.J., 1956. Physical properties of end-members of the garnet group. Am. Mineral. 41, 428–436.

Suzuki, I., Anderson, O.L., 1983. Elasticity and thermal expansion of a natural garnet up to 1000 K. J. Phys. Earth 31, 125–138.

Wang, Y., Gasparik, T., Liebermann, R.C., 1993. Modulated microstructure in synthetic majorite. Am. Mineral. 78, 1165–1173.

Wang, Y., Weidner, D.J., Liebermann, R.C., Zhao, Y., 1994. Thermal equation of state of (Mg,Fe)SiO_3 perovskite and constraints on composition of the lower mantle. Phys. Earth Planet. Int. 83, 13–40.

Wang, Y., Weidner, D.J., Guyot, F., 1996. Thermal equation of state of $CaSiO_3$ perovskite. J. Geophys. Res. 101, 661–672.

Wang, Y., Weidner, D.J., Meng, Y., 1997. Advances in equation of state measurements in SAM-85. In: Syono, Y., Manghnani. M.H. (Eds.), High Pressure Research: Application to Earth and Planetary Sciences, Am. Geophys. Union, Washington, DC, in press.

Wang, Y., Getting, I., Weidner, D.J., Vaughan, M.T., 1997. Performance of tapered anvils in DIA-type cubic anvil high pressure apparatus for X-ray diffraction studies. In: Syono, Y., Manghnani, M.H. (Eds.), High Pressure Research: Application to Earth and Planetary Sciences, Am. Geophys. Union, Washington, DC, in press.

Weidner, D.J., Vaughan, M.T., Ko, J., Wang, Y., Liu, X., Yeganeh-Haeri, A., Pocalo, R.E., Zhao, Y., 1992. Characterization of stress, pressure, and temperature in SAM85, a DIA type high pressure apparatus. In: Syono, Y., Manghnani, M.H. (Eds.), High Pressure Research: Applications to Earth and Planetary Sciences, Am. Geophys. Union, Washington, DC, pp. 13–17.

Weidner, D.J., Wang, Y., Vaughan, M.T., 1994. Yield strength at high pressure and temperature. Geophys. Res. Lett. 21, 753–756.

Yagi, T., Akaogi, M., Shimomura, O., Tamai, H., Akimoto, S., 1987. High pressure and high temperature equations of state of majorite. In: Syono, Y., Manghnani, M.H. (Eds.), High Pressure Research in Mineral Physics. Terrapub, Tokyo, pp. 141–147.

Yagi, T., Uchiyama, Y., Akaogi, M., Ito, E., 1992. Isothermal compression curve of $MgSiO_3$ tetragonal garnet. Phys. Earth Planet. Int. 74, 1–7.

Yeganeh-Haeri, A., Weidner, D.J., Ito, E., 1990. Elastic properties of the pyrope–majorite solid solution series. Geophys. Res. Lett. 17, 2453–2456.